JGR Planets

RESEARCH ARTICLE
10.1029/2022JE007221

Key Points:

- We study viscous relaxation of Pluto's impact-deformed ice shell and evolution of gravity anomaly associated with Sputnik Planitia basin
- Stress-dependent rheology can substantially speed up relaxation of the ice shell, while impact heating has only a minor effect
- The positive gravity anomaly responsible for the basin's position can be preserved only if the ice shell is thin (~100 km) or the ocean salty

Supporting Information:

Supporting Information may be found in the online version of this article.

Correspondence to:

M. Kihoulou,
kihoulou@karel.troja.mff.cuni.cz

Citation:

Kihoulou, M., Kalousová, K., & Souček, O. (2022). Evolution of Pluto's impact-deformed ice shell below Sputnik Planitia basin. *Journal of Geophysical Research: Planets*, *127*, e2022JE007221. https://doi.org/10.1029/2022JE007221

Received 28 JAN 2022
Accepted 9 MAY 2022

Evolution of Pluto's Impact-Deformed Ice Shell Below Sputnik Planitia Basin

M. Kihoulou[1], K. Kalousová[1], and O. Souček[2]

[1]Department of Geophysics, Faculty of Mathematics and Physics, Charles University, Prague, Czech Republic, [2]Mathematical Institute of Charles University, Faculty of Mathematics and Physics, Charles University, Prague, Czech Republic

Abstract Sputnik Planitia basin, the dominant surface feature of the dwarf planet Pluto, is located very close to the far point of Pluto-Charon tidal axis. This position is currently believed to be a result of whole body reorientation driven by the combination of (a) the uplift of a subsurface ocean in response to a basin-forming impact and (b) the nitrogen layer accumulated inside the basin. Since an ice shell made of pure water ice cannot maintain the uplift on timescales of billions of years, the presence of an insulating and highly viscous layer of methane clathrates at the base of the shell has recently been proposed. In this study, we solve the thermo-mechanical evolution of the ice shell in a 2D spherical axisymmetric geometry and evaluate the gravity anomaly associated with the evolving ice shell shape. Taking into account the effect of impact heating and stress-dependent rheology of both ice and clathrates, we show that a thick shell (≥200 km) loses the impact heat slowly which leads to fast uplift relaxation of the order of hundreds of million years. On the contrary, a thin shell (~100 km) cools down quickly (~10 Myr), becoming rigid and more likely to preserve the ocean/shell interface uplift till the present. These results suggest that a thick ocean may be present beneath Pluto's ice shell.

Plain Language Summary Several icy bodies within our Solar System are believed to have harbored a subsurface ocean below an outer ice shell early in their history. During a few billions of years (Solar System age), such oceans are likely to freeze, unless supplied by additional energy sources or chemical compounds that slow down the crystallization processes. In 2015, the New Horizons mission revealed signs that the dwarf planet Pluto may have also harbored a subsurface ocean. Moreover, the unlikely position of Pluto's dominant surface feature, Sputnik Planitia basin, assumed to be formed by a giant impact, suggests that Pluto's deep ocean may still be present. One of the hypotheses explaining the basin's position assumes that the ocean/shell boundary below the basin is deformed and that its shape is stable on long timescales due to presence of a layer of highly rigid and thermally insulating clathrates. In this paper, we study the effects of more realistic rheology than assumed previously as well as those of heating due to the impact that formed the basin. We show that a rather thin ice shell (~100 km) is more plausible than thicker shells thus implying that Pluto's ocean may be surprisingly thick (~200 km).

1. Introduction

Pluto is a dwarf planet with a radius of 1,188 km (Nimmo, Umurhan, et al., 2016), located in the Kuiper Belt. Most of what we currently know comes from the spectacular New Horizons flyby in 2015 (for a review, see e.g., Moore et al., 2016; Stern et al., 2015, 2018). Pluto's surface is mainly covered by water ice with traces of volatiles such as methane, nitrogen and carbon oxide (Grundy et al., 2016). The dominant feature of the surface is Sputnik Planitia, a vast, heart-shaped basin likely of impact origin (Greenstreet et al., 2015) and filled with a layer of solid nitrogen ice, probably several kilometers thick (McKinnon et al., 2017; Trowbridge et al., 2016). Pluto's interior is expected to be differentiated into a rocky core and a hydrosphere of about 300 km in thickness (McKinnon et al., 2017). Although the thermal structure of the hydrosphere is not well constrained, several lines of evidence suggest that a subsurface ocean has been present in Pluto's interior.

The existence of a liquid subsurface ocean was first proposed by Robuchon and Nimmo (2011), based on energy balance considerations that included the heat from radioactive decay, accretion, despinning and differentiation. After the New Horizons flyby, new observations supported the presence of an ocean, namely the absence of a detectable fossil bulge (Nimmo, Umurhan, et al., 2016) or numerous extensional faults suggestive of freezing of a liquid water beneath the ice shell (Bierson et al., 2020; Keane et al., 2016). Recent simulations by Denton

et al. (2020) who model the formation of Sputnik Planitia by an impact and track the resulting stress waves through Pluto also support the hypothesis.

The presence of an ocean also provides an explanation for the current position of Sputnik Planitia. A random impact location close to the tidal axis has been shown to be very unlikely (<10%) by Keane et al. (2016). Moreover, an impact basin without additional physical mechanism would produce a negative gravity anomaly, making the basin migrate toward the rotational axis by a whole-body reorientation (Matsuyama et al., 2014). Alternatively, if a global ocean was present, the negative gravity signal of the basin would be compensated by an isostatic uplift of the ocean below the basin. Provided that this process would be accompanied by surface accumulation of nitrogen in the basin, the resulting gravity anomaly would be positive (Nimmo, Hamilton, et al., 2016). Consequently, irrespective of the actual origin of the basin, whole-body reorientation in this case would lead to migration of Sputnik Planitia toward its present position close to the equator (Matsuyama et al., 2014). Additionally, in order to maintain Sputnik Planitia near the tidal axis over 4 Gyr (estimated age of the basin, Greenstreet et al. (2015)), the gravity anomaly has to stay positive, thus requiring the ocean uplift to remain unrelaxed, which is only possible if the ice shell is sufficiently rigid. This assumption may be problematic given the high temperature and therefore low viscosity at the ocean/shell interface. Any interface topography would thus be rapidly relaxed (∼100 Myr) by the induced lateral ice flow (Cadek et al., 2017). To overcome this issue, Kamata et al. (2019) suggested that a thin layer of methane clathrates could be present at the bottom of the ice shell (the interface with the ocean). Since clathrates have lower thermal conductivity than ice (Waite et al., 2007), they insulate the shell above them making the ice colder and thus more rigid. Moreover, clathrates themselves have higher viscosity than pure water ice close to the melting temperature (Durham et al., 2003). A combination of these two effects may significantly slow down the relaxation of the ocean uplift.

In the present paper, we study the thermal and mechanical evolution of an impact-deformed ice shell in a 2D axisymmetric spherical geometry with an evolving ocean/shell interface. Following Monteux et al. (2007), Monteux et al. (2014), we introduce thermal and topographic effect of an impact to estimate the initial temperature distribution and uplift dimensions. Because of large stresses generated within the ice shell, we employ a nonlinear stress-dependent viscous rheology. We discuss our results not only in terms of topography, but also in terms of the associated gravity anomaly, which controls the reorientation. The text is organized in the following way. In Section 2, we describe the mathematical model and its numerical implementation. In Section 3, we present the results obtained from simulations. Finally, we discuss our results and conclude this study in Sections 4 and 5, respectively.

2. Numerical Model

In order to estimate for how long the gravity anomaly generated by Sputnik Planitia could remain positive, we solve numerically the thermal and mechanical evolution of an impact-deformed ice shell in a 2D axisymmetric spherical geometry (Figure 1). We combine the rheology and thermal properties of water ice and methane clathrates, which were suggested to insulate the shell from below (Kamata et al., 2019), and we also take into account the effect of impact heating. The resulting gravity anomaly is calculated based on the topographies of individual density discontinuities: the ocean/shell interface (water/ice), the basin floor (ice/nitrogen) and the surface (nitrogen/vacuum). Note that for the sake of simplicity, we assume that the thickness of the nitrogen layer does not evolve in time and equals its current thickness 7 km (e.g., Nimmo, Hamilton, et al. (2016)). This approach provides an upper bound on the time during which the gravity anomaly remains positive and is also in accord with the expected fast accumulation of nitrogen in the basin on the time scale of only millions of years (Hamilton et al., 2016).

2.1. Governing Equations

To model the thermo-mechanical evolution of Pluto's ice shell with the clathrate layer at its bottom boundary, we use the following set of mass, momentum and energy balance equations for an incompressible non-Newtonian heat-conducting fluid in the Boussinesq approximation

$$0 = \nabla \cdot \boldsymbol{v}, \tag{1}$$

$$\mathbf{0} = -\nabla p + \nabla \cdot \eta \left(\nabla \boldsymbol{v} + \nabla^T \boldsymbol{v}\right) + \rho \left[1 - \alpha \left(T - T_r\right)\right] \boldsymbol{g}, \tag{2}$$

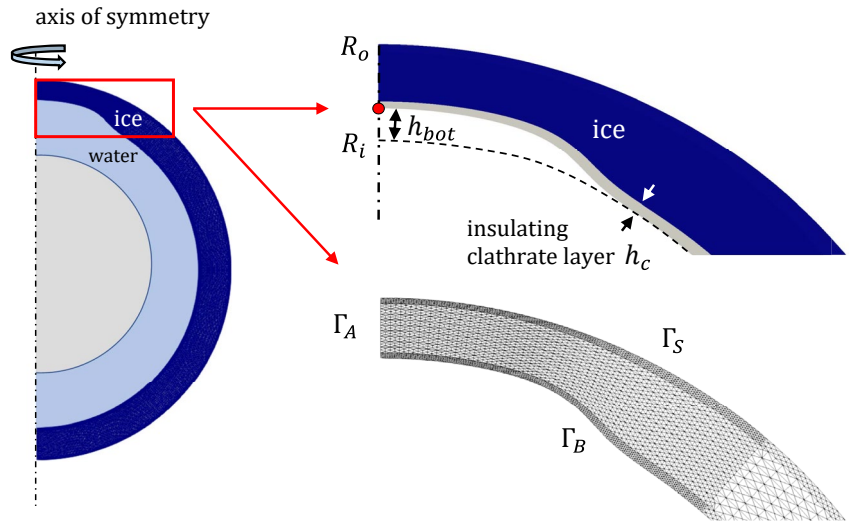

Figure 1. Left: Problem geometry. We address only the ice shell evolution (dark blue). Ocean uplift generated by the impact is located at the north pole. **Right top**: Detail of the problem geometry: Ice (dark blue) and clathrates (gray). The red point marks the ocean uplift center whose time evolution is investigated in Section 3. **Right bottom**: Computational mesh and the domain boundaries. The mesh is refined near the uplift area and at the top and bottom boundaries, where steep gradients of variables or material properties are expected.

$$\rho c_p \left(\frac{\partial T}{\partial t} + \boldsymbol{v} \cdot \nabla T \right) = \nabla \cdot (k \nabla T). \tag{3}$$

Here $\boldsymbol{v}$ denotes the velocity, p is the pressure, η is the viscosity, ρ is the density at reference temperature T_r, α is the thermal expansion coefficient, $\boldsymbol{g}$ is the gravity, c_p is the specific heat, and k is the thermal conductivity. The evolution of the ocean uplift topography h_{bot} is governed by the following equation

$$\frac{\partial h_{\text{bot}}}{\partial t} = v_r - (\nabla h_{\text{bot}} \cdot \boldsymbol{e}_\theta)\, v_\theta, \tag{4}$$

where v_r and v_θ are velocity components with respect to the local orthonormal (polar) system ($\boldsymbol{e}_r$, $\boldsymbol{e}_\theta$). The surface topography is assumed fixed throughout the simulations (for discussion see Section 2.4).

2.2. Material Properties

As described above, we assume that a clathrate layer of thickness h_c is present at the bottom interface of the ice shell with the ocean. To describe its position, we define an auxiliary function ϕ

$$\phi(R, \theta, t) = \frac{1}{2} \left[\tanh \left(-\frac{R - (R_i + h_c + h_{\text{bot}}(\theta, t)}{100 \text{ m}} \right) + 1 \right], \tag{5}$$

where R is the distance from Pluto's center and R_i is the radius of the ocean/shell interface, see Figure 1. Function ϕ smoothly changes from one in the clathrate layer to 0 in the rest of the ice shell in order to discriminate between the two material domains and the corresponding material parameters (thermal conductivity, viscosity). Thus defined, the clathrate layer has a constant thickness h_c and follows the shape of the bottom boundary (Figure 1, right top, gray area).

The effect of the clathrate layer at the ocean/shell interface is implemented via thermal conductivity and viscosity. The density of clathrates does not differ significantly from the ice density (Waite et al., 2007), thus we only use one value of ρ (see Table 2). Similarly, the heat capacity of clathrates at the ice melting temperature (clathrates are only present at the ocean/shell interface) is close to that of ice (Waite et al., 2007). For that reason, we do not distinguish between the ice and clathrate value and prescribe a temperature-dependent heat capacity (McCord & Sotin, 2005)

Table 1
Parameters for Ice and Clathrate Deformation Mechanisms (Durham et al., 2003; Goldsby & Kohlstedt, 2001)

Ice (stress-independent)				
	D_0 ($m^2 \cdot s^{-1}$)			Q ($kJ \cdot mol^{-1}$)
Volume diffusion	$9.1 \cdot 10^4$			59.4
Grain boundary diffusion	$6.4 \cdot 10^4$			49
Ice (stress-dependent)				
	A ($Pa^{-n} \cdot m^p \cdot s^{-1}$)	n	p	Q ($kJ \cdot mol^{-1}$)
Dislocation ($T < 258$ K)	$4.0 \cdot 10^{-19}$	4.0	0.0	60
Dislocation ($T > 258$ K)	$6.0 \cdot 10^4$	4.0	0.0	180
GBS ($T < 255$ K)	$6.2 \cdot 10^{-14}$	1.8	1.4	49
GBS ($T > 255$ K)	$5.6 \cdot 10^{15}$	1.8	1.4	192
BS	$2.2 \cdot 10^{-7}$	2.4	0.0	60
Clathrates (stress-dependent)				
BS	$2.24 \cdot 10^{-5}$	2.2	0.0	60

$$c_p(T) = a + bT, \tag{6}$$

where $a = 185\ J \cdot kg^{-1} \cdot K^{-1}$ and $b = 7.037\ J \cdot kg^{-1} \cdot K^{-2}$. We assume a temperature-dependent thermal conductivity of ice (Carnahan et al., 2021)

$$k_{ice}(T) = \frac{612\ W \cdot m^{-1}}{T}, \tag{7}$$

and, for the sake of simplicity, we use a constant value of clathrate thermal conductivity. Taking into account temperature and pressure conditions beneath the ice shell of Pluto, we adopt values $k_{clath} = 0.64$ and $0.66\ W \cdot m^{-1} \cdot K^{-1}$ for a 100 and 200 km thick ice shell, respectively, which are at melting temperature (265 K) almost 4× smaller than the value of ice thermal conductivity (Waite et al., 2007). The thermal conductivity in the shell can be then expressed in terms of the auxiliary function ϕ

$$k = k_{ice}(1 - \phi) + k_{clath}\phi, \tag{8}$$

so that $k = k_{clathr}$ in the clathrate layer ($\phi = 1$) and $k = k_{ice}$ in the rest of the ice shell ($\phi = 0$).

On timescales of millions of years, ice deforms by viscous flow which is accommodated by at least four known deformation mechanisms – diffusion creep, dislocation creep, grain boundary sliding and basal slip (Goldsby & Kohlstedt, 2001). These mechanisms are in general functions of temperature, grain size and stress and can be described by separate viscosity functions. For diffusion creep, we use a combination of volumetric and boundary diffusion (Goldsby & Kohlstedt, 2001)

$$\eta_{diff} = \frac{RTd^2}{84V_m}\left[D_{0,v}\exp\left(-\frac{Q_v}{RT}\right) + \frac{\pi\delta}{d}D_{0,b}\exp\left(-\frac{Q_b}{RT}\right)\right]^{-1}, \tag{9}$$

where R is the universal gas constant, d is the grain size, $D_{0,v}$ and $D_{0,b}$ along with Q_v and Q_b are the preexponential factors and activation energies for volume and boundary diffusion, respectively. Finally, $V_m = 1.97 \cdot 10^{-5}\ m^3$ is the molar volume and $\delta = 9.04 \cdot 10^{-10}$ m is the grain boundary width. Values of diffusion creep parameters are listed in Table 1. In the case of stress-dependent deformation mechanisms (dislocation creep, grain boundary sliding and basal slip), viscosity can be expressed as

$$\eta_i = \frac{1}{2}A_i^{-1/n_i}d^{p_i/n_i}\dot{\varepsilon}_{II}^{(1-n_i)/n_i}\exp\left(\frac{Q_i}{n_iRT}\right), \tag{10}$$

Table 2
Model Parameters

Variable	Symbol	Value	Unit
Outer radius	R_o	1188	km
Gravity	g	0.617	$m \cdot s^{-2}$
Ice shell thickness	H	100, 200	km
Clathrate layer thickness	h_c	5, 10	km
Ice density	ρ	917	$kg \cdot m^{-3}$
Ocean density	ρ_w	1100	$kg \cdot m^{-3}$
Nitrogen density	ρ_{N_2}	1000	$kg \cdot m^{-3}$
Surface temperature	T_{top}	40	K
Ocean/shell interface temperature	T_{bot}	265	K
Bond albedo	A	0.79	-
Ice emissivity	ε	0.97	-
Stefan-Boltzmann constant	σ	$5.67 \cdot 10^{-8}$	$W \cdot m^{-2} \cdot K^{-4}$
Solar constant	S	1360	$W \cdot m^{-2}$
Pluto's mean distance from the Sun	$R_\mathbb{P}$	39.5	AU
Grain size	d	1	mm
Cut-off viscosity	η_{max}	10^{24}	$Pa \cdot s$
Impactor velocity	v_{imp}	4	$km \cdot s^{-1}$
Impactor diameter	d_{imp}	400	km
Impactor density	ρ_{imp}	920	$kg \cdot m^{-3}$
Impact heating efficiency	γ	0.4	–
Attenuation exponent	m	3.4	–
Factor of effectively heated volume	h_m	5.8	–

where i denotes the particular deformation mechanism, $i \in \{disl, GBS, BS\}$, A_i is the preexponential factor, Q_i is the activation energy, p_i is the grain size exponent, $\dot{\varepsilon}_{II}$ is the strain rate invariant given by $\dot{\varepsilon}_{II} = \sqrt{\dot{\boldsymbol{\varepsilon}} : \dot{\boldsymbol{\varepsilon}}/2}$ and n_i is its exponent. Parameters for these mechanisms are listed in Table 1. All mechanisms can be combined to describe an effective viscosity η_{eff} by the following formula (Goldsby & Kohlstedt, 2001)

$$\frac{1}{\eta_{eff}} = \frac{1}{\eta_{diff}} + \frac{1}{\eta_{disl}} + \frac{1}{\eta_{GBS} + \eta_{BS}} + \frac{1}{\eta_{max}}, \tag{11}$$

where we introduced the cut-off viscosity η_{max} which bounds the viscosity from above for numerical reasons.

According to Durham et al. (2003), clathrates deform by basal slip (with viscosity given by Equation 10). Values of viscosity parameters appropriate for clathrates are given in Table 1. Due to a large contrast between the clathrates and ice viscosities, we use their power-law combination

$$\eta = \eta_{eff}^{1-\phi} \eta_{clath}^{\phi}. \tag{12}$$

In cases where the stress-dependent rheology is not considered, we use diffusion creep (Equation 9) as the only mechanism.

2.3. Post-Impact Thermal State and Topography

The collision of a smaller body (impactor) with a larger one (target), considered to be the formation mechanism for Sputnik Planitia, has several consequences. First, the total energy must be conserved and thus part the of impactor's kinetic energy is transformed into internal energy which leads to a local increase of the target's temperature. If the impactor velocity v_{imp} is larger than the seismic velocities of the target, a shock wave develops (Croft, 1982). The associated temperature increase ΔT is then nearly uniform in a spherical region of radius R_{ic}–the isobaric core–located below the impact center and strongly decays away from it (Senshu et al., 2002). The radius of the isobaric core R_{ic} is usually considered to be proportional to the impactor radius r_{imp} with a factor of $\sqrt[3]{3}$, that is, $R_{ic} \propto \sqrt[3]{3}\, r_{imp}$ (Monteux et al., 2007).

Let us assume that the kinetic energy E_k of the impactor of the volume V_{imp} is transformed with efficiency γ into the internal energy of the target E_i

$$\gamma E_k \equiv \gamma \frac{1}{2} \rho_{imp} V_{imp} v_{imp}^2 = E_i \equiv Q V_{eff}, \tag{13}$$

where ρ_{imp} is the impactor density and Q is the amount of heat per unit volume obtained by the effectively heated volume V_{eff} of the target. Denoting h_m the ratio of the volume V_{eff} to the volume of the isobaric core

$$h_m = \frac{V_{eff}}{V_{ic}} \sim \frac{V_{eff}}{3V_{imp}}, \tag{14}$$

(due to proportionality of R_{ic} and r_{imp}, see above), the heat per unit volume Q can be expressed as

$$Q = \frac{1}{6} \frac{\rho_{imp} v_{imp}^2}{h_m} \gamma. \tag{15}$$

The value of γ is typically considered to be between 0.2 and 0.6 (Monteux et al., 2014), while the value of h_m is determined by the attenuation exponent m defined below, see Monteux et al. (2007) for further details. The resulting post-impact temperature increase ΔT can then be estimated as

$$\Delta T = \frac{-a + \sqrt{a^2 + 2b\left(Q/\rho + aT_0 + bT_0^2/2\right)}}{b} - T_0, \tag{16}$$

where T_0 is the pre-impact temperature profile, see Supporting Information S1 for details. The constants a and b represent the constant and linear term, respectively, in Equation 6. The post-impact temperature field can be expressed as

$$T(r) = \begin{cases} T_0 + \Delta T & \text{for } r < R_{\text{ic}}, \\ T_0 + \Delta T \left(\frac{R_{\text{ic}}}{r} \right)^m & \text{for } r \geq R_{\text{ic}}, \end{cases} \tag{17}$$

with the attenuation exponent, m, typically assumed to be between 2.8 and 4.0 (Monteux et al., 2014). The particular values of parameters γ, m, and h_m used in the present study are given in Table 2.

Second, the impactor excavates the target material, creating a transient crater whose walls collapse forming the final crater (Zahnle et al., 2003). Its diameter can be estimated using the following scaling law (see Equation A6 in Zahnle et al. (2003))

$$D = a_0 \left(\frac{v_{\text{imp}}}{v_{\text{esc}}} \right)^{2a_1} \left(\frac{\rho_{\text{imp}}}{\rho_{\text{tar}}} \right)^{a_2} R_{\text{tar}}^{a_3} \left(2R_{\text{imp}} \right)^{a_4} \cos^{a_5} \left(\vartheta_{\text{inc}} \right), \tag{18}$$

where v_{esc} is the target escape velocity, R_{imp}, ρ_{imp} and R_{tar}, ρ_{tar} are the radius and density of the impactor and the target, respectively. We choose the angle of incidence ϑ_{inc} to be 0° as in Senft and Stewart (2008), providing an upper bound for D (see Equation 18) for a given impactor. Let us note, that it does not represent the most probable value that would be 45° (Kraus et al., 2011). The values of scaling parameters a_i are as follows: $a_0 = 1.1$, $a_1 = 0.217$, $a_2 = 0.333$, $a_3 = 0.217$, $a_4 = 0.783$, and $a_5 = 0.44$ (Zahnle et al., 2003). Fixing the impactor velocity allows us to estimate suitable combinations of impactor density and diameter. According to Kohnen (1974), the P-wave velocity at 40 K (Pluto's surface temperature) is approximately 4 km $\cdot$ s^{-1} and decreases with temperature (and thus depth, see also Vance et al. (2018)). In order to satisfy the condition for the shock wave development mentioned above, we will use $v_{\text{imp}} = 4$ km $\cdot$ s^{-1}. Note that the average impactor velocity at Pluto is expected to be about 2 km $\cdot$ s^{-1} (Zahnle et al., 2003). For such low velocity, a shock wave would, however, not develop and, consequently, the post-impact temperature increase would be negligible – this scenario is already included in the models without impact heating (see Section 3). In order to assess the role of possible impact heating, we picked the smallest value of impact velocity that would result in impact heating.

Assuming further an impactor of density 920 kg $\cdot$ m^{-3} (Johnson et al., 2016) and basin diameter 1,000 km (Nimmo, Hamilton, et al., 2016), Equation 18 gives impactor diameter of ~400 km, which is in agreement with, for example, Denton et al. (2020). Values of all parameters are given in Table 2.

2.4. Boundary and Initial Conditions

The boundary of the computational domain consists of three parts: the bottom boundary Γ_B (interface with the ocean), the surface boundary Γ_S and the axis of symmetry Γ_A (Figure 1, right bottom). We prescribe fixed temperature at the bottom boundary and zero normal heat flux at the axis of symmetry.

$$T|_{\Gamma_B} = T_o, \tag{19}$$

$$(\boldsymbol{q} \cdot \boldsymbol{n})|_{\Gamma_A} = 0, \tag{20}$$

where $\boldsymbol{q} = -k\nabla T$ denotes the heat flux, $\boldsymbol{n}$ is the unit vector normal to the boundary and T_o is the ocean temperature. On the top boundary, we prescribe either radiation condition (for models with impact heating, see Section 3) or fixed temperature (otherwise)

$$(\boldsymbol{q} \cdot \boldsymbol{n})_{\Gamma_S} = \frac{S}{\left(R_{\text{♇}} / R_{\oplus} \right)^2} (1 - A) - \varepsilon \sigma T^4 \tag{21a}$$

or

$$T|_{\Gamma_S} = T_S, \tag{21b}$$

respectively, where S denotes the Solar constant, $R_{\text{♇}}$ and $R_{\oplus}$ are mean distances of Pluto and the Earth from the Sun, respectively, σ denotes the Stefan-Boltzmann constant, ε is the ice emissivity, A is the Bond albedo of Pluto's surface and T_S is the surface equilibrium temperature.

For the momentum equation, we use a free-slip boundary condition at the surface and the axis of symmetry.

$$(\boldsymbol{v} \cdot \boldsymbol{n})|_{\Gamma_{A \cup S}} = 0, \tag{22}$$

$$\left(\boldsymbol{\tau}^D \cdot \boldsymbol{n}\right)_t |_{\Gamma_{A \cup S}} = \boldsymbol{0}, \tag{23}$$

where $\boldsymbol{\tau}^D$ is the deviatoric part of Cauchy stress tensor, $\boldsymbol{\tau} = -p\boldsymbol{I} + \boldsymbol{\tau}^D$. On the bottom boundary, we prescribe (hydrostatic) ocean pressure

$$(\boldsymbol{\tau} \cdot \boldsymbol{n})|_{\Gamma_B} = p_{\text{ocean}} \boldsymbol{n}, \tag{24}$$

where $p_{\text{ocean}} = g(H\rho_{\text{i}} - \rho_{\text{w}} h_{\text{bot}})$ and H is the (reference) shell thickness, see Table 2.

The lateral dimensions (∼1,000 km) and initial depth (∼10 km) of the surface basin are adopted from Nimmo, Hamilton, et al. (2016). In our axially symmetric model, the crater center is located at the north pole ($\theta = 90°$) and we can thus define the surface basin topography as a function of latitude θ (in degrees)

$$h_{\text{top}}(\theta) = -10 \text{ km} \left(\frac{1 + \tanh\left(\frac{\theta - 68.5°}{5°}\right)}{2} \right). \tag{25}$$

The surface basin topography h_{top} is not evolved in our simulations, since the values of the estimated basin depth after the impact and the present depth are very close (e.g., Nimmo, Hamilton, et al., 2016; Trowbridge et al., 2016; McKinnon et al., 2017), suggesting that no significant surface relaxation has taken place. The basin topography is thus only used to (a) evaluate the gravity anomaly (see Equation 11 in Supporting Information S1) and to (b) estimate the initial ocean/shell boundary uplift. For this, we employ the assumption of Airy isostasy (Airy, 1855; Bursa & Pec, 2013; Cadek et al., 2019) using the findings by Johnson et al. (2016) that a positive gravity anomaly can only be obtained if the ocean density is higher than ∼1,100 kg · m^{-3}. This value, which we adopt in our study, can be the result of 5%–10% $MgSO_4$ dissolved in Pluto's ocean (Vance et al., 2018). Note that $MgSO_4$ is often present in CI and CM chondrites (Hogenboom et al., 1995), whose composition is considered representative of the primordial building material.

As an initial condition for temperature, we prescribe a conductive temperature field evaluated using the shell (clathrate/ice) conductivity (Equation 8). Since for the chosen ice shell/clathrate layer thicknesses (100/5 and 200/10 km) the conductive cooling timescales are less than 100 Myr (see Figure S1 in Supporting Information S1), we assume that the shell was cooled down due to the insulating effect of clathrates already before the impact. For simulations with impact heating, this conductive temperature field is overlaid by the thermal anomaly estimated from Equation 16.

2.5. Numerical Method

We solve the set of governing equations equipped with the material parameters and boundary conditions by a Finite Element Method, implemented in the open-source platform FEniCS (Alnæs et al., 2015; Logg et al., 2012). We employ a structured triangular mesh refined near the ocean/shell interface as well as at the top boundary (see Figure 1, right bottom). For the discretization of the Stokes problem (Equations 1 and 2), we use the Taylor-Hood elements–quadratic for velocity and linear for pressure (Taylor & Hood, 1973), for energy balance (Equation 3) quadratic elements and for the kinematic equation (Equation 4) linear elements. The energy balance and the kinematic equation that contain the time derivative are discretized by the Crank-Nicolson and implicit Euler scheme, respectively. The code was extensively tested against a spectral method solution and a solution obtained by commercial FEM software COMSOL 3.5a. To evaluate the gravity anomaly at the surface, we use a spectral method (Cadek et al. (2021), see SI for details) and parameters listed in Table 2.

Table 3
List of Performed Simulations

Model	H (km)	h_c (km)	CR	IH
1a	**100**	**5**	**yes**	**yes**
1b	100	5	yes	no
1c	100	5	no	yes
1d	100	5	no	no
2a	**200**	**10**	**yes**	**yes**
2b	200	10	yes	no
2c	200	10	no	yes
2d	200	10	no	no

Note. Reference simulations (letter "a") with composite rheology (CR) and impact heating (IH) included are marked in bold. Simulations "b" and "c" investigate the effect of composite rheology and impact heating alone, respectively. Simulations "d" represent the setting of Kamata et al. (2019), that is, temperature-dependent viscosity only and no impact heating.

3. Results

We performed a series of simulations to investigate the effect of the main model parameters – the reference thickness of the ice shell (H) and of the clathrate layer (h_c), as well as the effect of the particular model setting – rheology and impact heating. For the thicknesses, we use the two end-member values, which, according to Kamata et al. (2019) lead to the slowest relaxation: $H = 100$ km combined with $h_c = 5$ km (models 1a–d, see Table 3) and $H = 200$ km combined with $h_c = 10$ km (models 2a–d). The distinct rheology and heating settings are denoted by letters "a" to "d" (see Table 3).

Figure 2 shows the evolution of viscosity for models 1a (left) and 2a (right) that include the effect of impact heating as well as nonlinear composite rheology (CR). The initial state (top row) shows locally decreased viscosity (red color) due to impact heating (isobaric core region). The middle row shows the simulations' results at $t = 1$ Myr. Since the thin shell (model 1a, left) contains only a small amount of warm ice, it cools down very quickly and at 1 Myr, it is already effectively rigid ($\eta > 10^{20}$ Pa · s). On the other hand, in the case of a thick shell (model 2a, right), the volume of the heated ice is larger and thus vigorous convection develops in the ice below the impact site. However, as the shell gradually loses heat, convection ceases even in the thicker shell–at the end of the simulation ($t = 4$ Gyr, bottom row), both shells

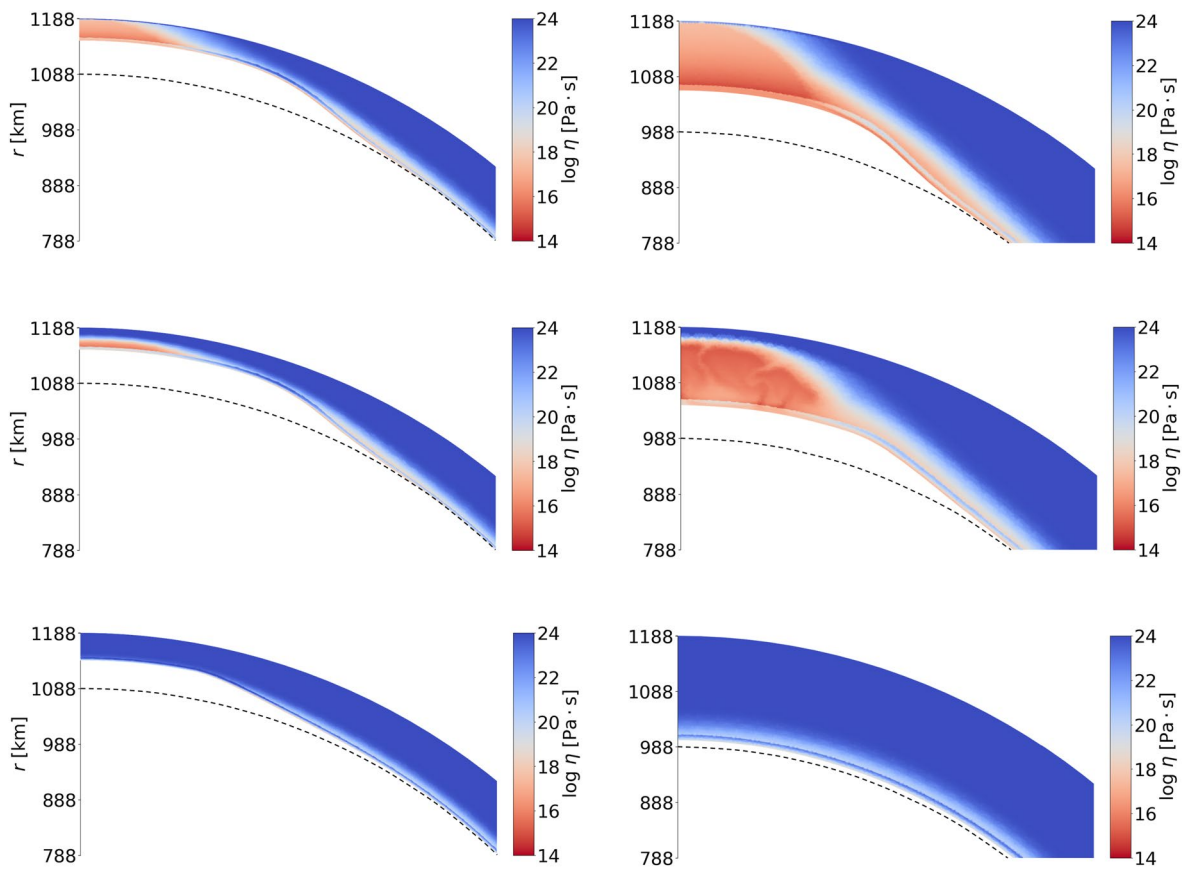

Figure 2. Evolution of viscosity (color) for models 1a (left) and 2a (right), r denotes the radial distance from Pluto's center, dashed line indicates the pre-impact ocean/shell boundary. **Top:** initial state ($t = 0$ Myr). Note local viscosity decrease (red color) due to impact heating. **Middle:** simulation results at $t \simeq 1$ Myr. The thinner shell (model 1a) cools quickly and thus becomes rigid, while the thicker shell (model 2a) remains warm below the impact location and enables development of local convection. **Bottom:** end of simulation ($t \simeq 4$ Gyr). In model 2a, the uplift is fully relaxed, while in model 1a the uplift subsided by only a few kilometers.

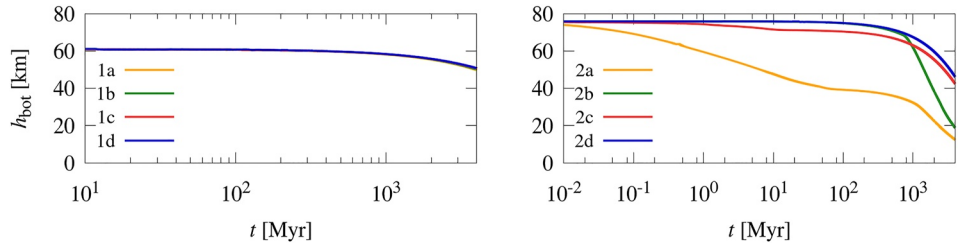

Figure 3. Time evolution of the ocean uplift center (h_{bot} at $\theta = 90°$, see text). Note that the time scale is logarithmic and its range differs between the left and the right panel. **Left:** Models with a thin shell ($H = 100$ km)–the effect of rheology or impact heating (IH) is negligible. **Right:** Models with a thick shell ($H = 200$ km)–combined IH + composite rheology (CR) (2a) as well as CR alone (2b) lead to significantly faster relaxation compared to the case without IH and with only temperature-dependent rheology (2d). The effect of IH alone (2c) is negligible.

are cold, rigid and purely conductive. But the state of the ocean/shell interface is quite different–while the thick shell relaxed completely and there is no sign of the initial ocean uplift (bottom right), the relaxation in the thin shell proceeded so slowly that a visible uplift is still present, even after 4 Gyr of simulation (bottom left).

Figure 3 shows the time evolution of the ocean uplift center (i.e., the intercept of the bottom boundary and the axis of symmetry, see the red point in Figure 1, right top). Models 1a and 2a (yellow color) correspond to the full setting (with both impact heating and composite rheology), whose relaxation was investigated in detail in Figure 2. While in the case of the thin shell ($H = 100$ km, left), the uplift center subsides by about 10 km (from 60 to 50 km), the uplift center in the thick shell ($H = 200$ km, right) sank by more than 60 km (from almost 80 to 10 km). This is in clear contrast to models with only temperature-dependent rheology and no impact heating (models 1d, 2d, blue color) that correspond to the setting used by Kamata et al. (2019). In those cases, the ocean uplift is not relaxed even after 4 Gyr of simulation, which is in agreement with Kamata et al.'s conclusions. To distinguish between the effects of composite rheology and impact heating, we also performed simulations with only one of these effects taken into account (1b and 2b–composite rheology only, 1c and 2c–impact heating only). If a composite rheology is employed, grain boundary sliding and basal slip lead to viscosity decrease in the vicinity of the uplift, where large stresses are present. Impact heating, on the other hand, decreases viscosity only at the beginning of the simulation and its effect is suppressed once the shell has cooled down.

In Figure 3, these effects are well demonstrated by the model with a thick shell ($H = 200$ km, right): the relaxation curve of the model with impact heating but only temperature-dependent rheology (2c, red color) differs from the cases without impact heating (2b and 2d) during the first ~10 Myr, but afterward, the relaxation rate is comparable to that of case 2d (no impact heating, temperature-dependent rheology, blue color). On the other hand, the relaxation curve of the model with composite rheology but no impact heating (2b, green color) follows closely that of model 2d (blue) till ~500 Myr, but then its rate changes abruptly, leading to almost full relaxation at the end of the simulation ($t = 4$ Gyr)–the remaining uplift is only about 20 km, similar to that for the full model (2a, yellow). Therefore, the inclusion of a composite rheology seems to have a more pronounced effect on the ocean uplift relaxation rate than the inclusion of impact heating. Models with a thin shell ($H = 100$ km, left) are much less sensitive to these effects although a small difference can be observed at the end of simulation for models with composite rheology (1a–yellow and 1b–green). However, the effect of stress-dependent mechanisms is reduced by the low temperatures. The ocean uplift in all thin shell models subsides by only about 10 km during 4 Gyr.

Figure 4 shows the time evolution of surface gravity anomaly at degree $j = 2$ generated by the uplift, the surface crater and the solid nitrogen within (see Supporting Information S1 for the details on its evaluation), which represents the change in Pluto's moment of inertia and is therefore responsible for its reorientation. In particular, the sign of the anomaly determines the direction of reorientation with negative values leading to poleward movement and positive values rotating the crater toward the equator. Results in the left panel show that all models with $H = 100$ km stay in positive values during the simulation. Therefore, the thin shell allows Sputnik Planitia to migrate toward and remain close to the equator. On the other hand, results for the thick shell ($H = 200$ km) show that the more realistic setting with composite rheology and impact heating leads to a change in the gravity anomaly sign during the relaxation. This indicates that if the shell is thick, Sputnik Planitia would eventually reorient toward the rotational axis.

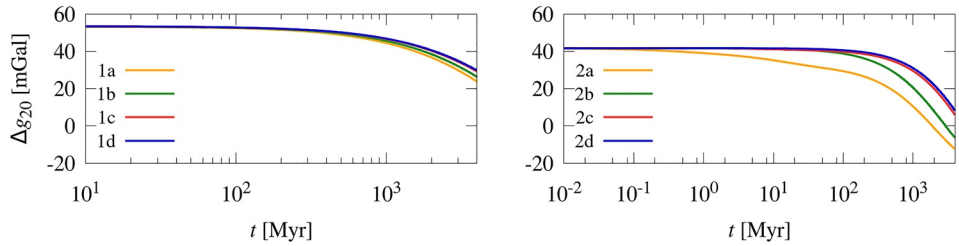

Figure 4. Time evolution of gravity anomaly at spherical harmonic degree $j = 2$ (see text). Note that the time scale is logarithmic and its range differs between the left and the right panel. **Left:** Models with a thin shell ($H = 100$ km)–the gravity anomaly stays positive for all cases. **Right:** Models with a thicker shell ($H = 200$ km)–simulations with more realistic (composite) rheology (2a and 2b) change sign before 4 Gyr.

4. Discussion

The results presented in Section 3 show that the relaxation rate of an impact-induced uplift strongly differs for the thin (∼100 km) and the thick (≥200 km) shell, since it depends on the internal thermal structure, which evolves in time. In the context of the hypothetical ocean uplift below Sputnik Planitia basin suggested by Kamata et al. (2019), our results indicate that Pluto's shell has to be thin (∼100 km) in order to maintain significant uplift topography on timescales of the order of 4 Gyr. However, several simplifications were made that should be considered before interpreting the results.

The formula for the temperature anomaly amplitude (Equation 16) was derived under the assumption that the lateral dimensions of the crater are negligible with respect to the shell thickness (Monteux et al., 2007, 2014). Regarding the diameter of Sputnik Planitia (1,000 km), which is three times larger than the thickness of the hydrosphere (327 km), such approach may not be accurate. Johnson et al. (2016) performed a series of numerical simulations of Sputnik Planitia basin formation and presented post-impact temperature fields with both surface and uplift topographies. According to their results, the ice shell is nearly molten through below the region of impact. In our case, the shell reached the melting temperature only at the very bottom, since we considered significantly colder pre-impact state because of the clathrates (see Supporting Information S1 for details).

Shell thickness appears to be a crucial parameter in the uplift relaxation problem. In our model, we considered that the thicknesses of both the ice shell and the clathrate layer are not affected by either melting or freezing. Such a choice in the case of the ice shell is reasonable–according to Kamata et al. (2019), in the presence of clathrates, the thickness of the ice shell does not vary significantly over 4 Gyr. The clathrates, however, may accumulate up to a few tens of kilometers thick layer (Kamata et al., 2019). On the other hand, immediately after the impact, the clathrate layer might have been much thinner than our model assumes. Recent impact simulations by Denton et al. (2020) show that the ice shell might have been locally disrupted by enormous excavation of the impact region, which makes the preservation of a uniform layer doubtful. For the lack of better knowledge, we adopted the thickness values that are, according to Kamata et al. (2019), the most favorable to slow down the uplift relaxation, that is, 5 and 10 km for 100 and 200 km thick ice shell, respectively. Investigation of other thicknesses or implementation of the clathrate layer evolution is left for another study.

The key parameter governing the relaxation is viscosity, which depends in general on the grain size, temperature and stress. The effect of stress was discussed in Section 3. Temperature at the ocean/shell interface equals the melting temperature, which can be reduced by tens of Kelvins if ammonia was present (Hogenboom et al., 1997). However, ammonia also reduces water density and its presence would thus make the gravity anomaly contribution insufficient for compensation, see for example, Johnson et al. (2016). The melting temperature can also be reduced by up to 20 K by the presence of salts such as NaCl or $MgSO_4$, which also increases water density (e.g., Vance et al., 2014, 2018), pronouncing the gravity effect of the ocean uplift. Lower ocean temperature will result in an increase in the ice/clathrate viscosity, and thus in slower relaxation. To assess the effect of a cold ocean, we performed additional simulations with ocean temperature set to 250 K–in such a setting, the gravity anomaly remains positive for at least 4 Gyr even in the case of a thick shell (see Text S4 and Figure S3 in Supporting Information S1). These results indicate that a thin and very salty ocean might also be admissible.

Finally, the grain size is a parameter that directly affects the viscosity, and therefore the relaxation rate. Since its value is unknown, a stable ocean uplift could be easily explained by sufficiently large ice grains. We chose a constant value of 1 mm, following the published studies (e.g., Barr & McKinnon 2007; McKinnon 1999 and many others). However, the ice grains experience both growth and reduction, depending on the presence of impurities and the deformation they are exposed to, therefore their size is a function of both space and time (Barr & McKinnon, 2007; Rozel et al., 2011). A significant grain growth in the vicinity of relaxing uplift seems to be unlikely, since dislocation creep, occurring at large stresses (produced e.g., by the uplift) reduces the grain size (Barr & McKinnon, 2007; Rozel et al., 2011). Another concern is that viscous rheology does not well describe the material behavior under conditions on the surface of icy bodies (low temperatures, high stresses) and elastic as well as brittle behavior should be considered which is however beyond the scope of this paper. For that reason, the evolution of the surface topography is not addressed in this work since, being much colder, it is also unrealistically rigid if one assumes only viscous behavior. Detailed simulations covering grain size evolution and more realistic rheology are left for a future study.

5. Conclusions

In the present study, we developed a 2D spherical axisymmetric model in order to investigate the relaxation of Pluto's impact-deformed ice shell underlain by an ocean. We studied the effect of impact heating and stress-dependent viscosity on the ocean uplift relaxation, while the shell was insulated from below by a high viscosity and low conductivity clathrate layer. We further evaluated the gravity anomaly at degree 2 resulting from the surface topography, nitrogen layer and uplift topography, and focused on the transition between the positive and negative values, that is, the tendency to reorient toward the equator and rotation axis, respectively.

We examined the relaxation of a thick (200 km) and a thin (100 km) shell with the initial uplift determined by an assumption of Airy isostasy. The thick shell is initially warm, therefore a temporary local convection occurs. Due to low ice viscosity, the shell undergoes a fast initial relaxation lasting up to 10 Myr, at which point convection ceases. A phase of stagnation follows after, lasting until approximately 1 Gyr, after which the relaxation continues, however, at much slower rate. In the case of pure water ocean, the associated gravity anomaly becomes negative after 2 Gyr. Assuming the Sputnik Planitia basin to be 4 Gyr old, its migration by whole-shell reorientation toward the equator cannot be explained by a pure water ocean uplift and a thick ice shell. However, the presence of antifreeze such as NaCl could significantly reduce the ocean temperature and slow down the relaxation, thus ensuring the gravity anomaly stays positive. When the shell is thin, it cools down quickly and convection does not develop. Therefore, there is no fast initial relaxation and the shell soon becomes cold and rigid. The resulting gravity anomaly remains positive for at least 4 Gyr. Overall, our study shows that a thin shell with a thick ocean is more likely to support the reorientation theory. Alternatively, a thin salty ocean is also consistent with the theory. Note that the assumption of a clathrate layer of uniform thickness constant in time along with the assumption of a constant grain size represent two major simplifications. Taking these two effects into account is non-trivial and would require a more detailed study.

Data Availability Statement

All data used for producing figures in the paper can be found on https://doi.org/10.5281/zenodo.6518892.

Acknowledgments
The authors would like to thank Francis Nimmo and an anonymous reviewer for their comments which helped to improve the manuscript, dr. Julien Monteux for his help with the parameterization of impact heating and prof. Ondřej Čadek for fruitful discussions on ice shell relaxation. This research was supported by the Czech Science Foundation through project No. 22-20388S. M.K. acknowledges the support from the Charles University project SVV-2021-260581 and project GA UK No. 355521. K.K. was supported by the Charles University Research program No. UNCE/SCI/023. All data used for producing figures in the paper can be found in Kihoulou et al. (2022).

References

Airy, G. B. (1855). On the computation of the effect of the attraction of mountain-masses, as disturbing the apparent astronomical latitude of stations in geodetic surveys. *Philosophical Transactions of the Royal Society of London*, *145*(2), 101–104. https://doi.org/10.1098/rstl.1855.0003

Alnæs, M., Blechta, J., Hake, J., Johansson, A., Kehlet, B., Logg, A., & Wells, G. N. (2015). The FEniCS project version 1.5. *Archive of Numerical Software*, *3*(100), 9–23. https://doi.org/10.11588/ans.2015.100.20553

Barr, A. C., & McKinnon, W. B. (2007). Convection in ice I shells and mantles with self-consistent grain size. *Journal of Geophysical Research*, *112*(E2), E02012. https://doi.org/10.1029/2006JE002781

Bierson, C., Nimmo, F., & Stern, S. (2020). Evidence for a hot start and early ocean formation on Pluto. *Nature Geoscience*, *13*(7), 468–472. https://doi.org/10.1038/s41561-020-0595-0

Bursa, M., & Pec, K. (2013). *Gravity field and dynamics of the Earth*. Springer Science & Business Media.

Cadek, O., Behounkova, M., Tobie, G., & Choblet, G. (2017). Viscoelastic relaxation of Enceladus's ice shell. *Icarus*, *291*, 31–35. https://doi.org/10.1016/j.icarus.2017.03.011

Cadek, O., Kalousova, K., Kvorka, J., & Sotin, C. (2021). The density structure of Titan's outer ice shell. *Icarus*, *364*, 114466. https://doi.org/10.1016/j.icarus.2021.114466

Cadek, O., Soucek, O., & Behounkova, M. (2019). Is airy isostasy applicable to icy Moons? *Geophysical Research Letters*, *46*(24), 14299–14306. https://doi.org/10.1029/2019GL085903

Carnahan, E., Wolfenbarger, N. S., Jordan, J. S., & Hesse, M. A. (2021). New insights into temperature-dependent ice properties and their effect on ice shell convection for icy ocean worlds. *Earth and Planetary Science Letters*, *563*, 116886. https://doi.org/10.1016/j.epsl.2021.116886

Croft, S. K. (1982). A first-order estimate of shock heating and vaporization in oceanic impacts. In *Geological implications of impacts of large Asteroids and Comets on the Earth*. Geological Society of America. https://doi.org/10.1130/SPE190-p143

Denton, C., Johnson, B., Wakita, S., Freed, A., Melosh, H., & Stern, S. (2020). Pluto's antipodal terrains imply a thick subsurface ocean and hydrated core. *Geophysical Research Letters*, *48*(2). https://doi.org/10.1029/2020GL091596

Durham, W., Kirby, S., Stern, L., & Zhang, W. (2003). The strength and rheology of methane clathrate hydrate. *Journal of Geophysical Research*, *108*(B4), 2182. https://doi.org/10.1029/2002JB001872

Goldsby, D., & Kohlstedt, D. (2001). Superplastic deformation of ice: Experimental observations. *Journal of Geophysical Research*, *106*(B6), 11017–11030. https://doi.org/10.1029/2000JB900336

Greenstreet, S., Gladman, B., & McKinnon, W. (2015). Impact and cratering rates onto Pluto. *Icarus*, *258*, 267–288. https://doi.org/10.1016/j.icarus.2015.05.026

Grundy, W., Binzel, R., Buratti, B., Cook, J., Cruikshank, D., Dalle Ore, C., et al. (2016). Surface compositions across Pluto and Charon. *Science*, *351*(6279), aad9189. https://doi.org/10.1126/science.aad9189

Hamilton, D., Stern, S., Moore, J., Young, L., Binzel, R. P., Buie, M. W., et al. (2016). The rapid formation of Sputnik Planitia early in Pluto's history. *Nature*, *540*(7631), 97–99. https://doi.org/10.1038/nature20586

Hogenboom, D., Kargel, J., Consolmagno, G., Holden, T., Lee, L., & Buyyounouski, M. (1997). The ammonia–water system and the chemical differentiation of icy satellites. *Icarus*, *128*(1), 171–180. https://doi.org/10.1006/icar.1997.5705

Hogenboom, D., Kargel, J., Ganasan, J., & Lee, L. (1995). Magnesium sulfate-water to 400 MPa using a novel piezometer: Densities, phase equilibria, and planetological implications. *Icarus*, *115*(2), 258–277. https://doi.org/10.1006/icar.1995.1096

Johnson, B. C., Bowling, T. J., Trowbridge, A. J., & Freed, A. M. (2016). Formation of the Sputnik Planum basin and the thickness of Pluto's subsurface ocean. *Geophysical Research Letters*, *43*(19), 10068–10077. https://doi.org/10.1002/2016GL070694

Kamata, S., Nimmo, F., Sekine, Y., Kuramoto, K., Noguchi, N., Kimura, J., & Tani, A. (2019). Pluto's ocean is capped and insulated by gas hydrates. *Nature Geoscience*, *12*(6), 407–410. https://doi.org/10.1038/s41561-019-0369-8

Keane, J., Matsuyama, I., Kamata, S., & Steckloff, J. (2016). Reorientation and faulting of Pluto due to volatile loading within Sputnik Planitia. *Nature*, *540*(7631), 90–93. https://doi.org/10.1038/nature20120

Kihoulou, M., Kalousová, K., & Souček, O. (2022). Evolution of Pluto's impact-deformed ice shell below Sputnik Planitia basin (data). *Zenodo*. https://doi.org/10.5281/zenodo.6518892

Kohnen, H. (1974). The temperature dependence of seismic waves in ice. *Journal of Glaciology*, *13*(67), 144–147. https://doi.org/10.3189/S0022143000023467

Kraus, R. G., Senft, L. E., & Stewart, S. T. (2011). Impacts onto H_2O ice: Scaling laws for melting, vaporization, excavation, and final crater size. *Icarus*, *214*(2), 724–738. https://doi.org/10.1016/j.icarus.2011.05.016

Logg, A., Mardal, K.-A., & Wells, G. (Eds.) (2012). *Automated solution of differential equations by the finite element method* (Vol. 84). Springer-Verlag Berlin Heidelberg. https://doi.org/10.1007/978-3-642-23099-8

Matsuyama, I., Nimmo, F., & Mitrovica, J. (2014). Planetary reorientation. *Annual Review of Earth and Planetary Sciences*, *42*(1), 605–634. https://doi.org/10.1146/annurev-earth-060313-054724

McCord, T. B., & Sotin, C. (2005). Ceres: Evolution and current state. *Journal of Geophysical Research*, *110*(E5), E05009. https://doi.org/10.1029/2004JE002244

McKinnon, W. B. (1999). Convective instability in Europa's floating ice shell. *Geophysical Research Letters*, *26*(7), 951–954. https://doi.org/10.1029/1999GL900125

McKinnon, W. B., Stern, S., Weaver, H., Nimmo, F., Bierson, C., Grundy, W., et al. (2017). Origin of the Pluto–Charon system: Constraints from the New Horizons flyby. *Icarus*, *287*, 2–11. https://doi.org/10.1016/j.icarus.2016.11.019

Monteux, J., Choblet, G., Tobie, G., & Le Feuvre, M. (2014). Can large icy moons accrete undifferentiated? *Icarus*, *237*, 377–387. https://doi.org/10.1016/j.icarus.2014.04.041

Monteux, J., Coltice, N., Dubuffet, F., & Ricard, Y. (2007). Thermo-mechanical adjustment after impacts during planetary growth. *Geophysical Research Letters*, *34*(24), L24201. https://doi.org/10.1029/2007GL031635

Moore, J., McKinnon, W., Spencer, J., Howard, A., Schenk, P., Beyer, R., et al. (2016). The geology of Pluto and Charon through the eyes of New Horizons. *Science*, *351*(6279), 1284–1293. https://doi.org/10.1126/science.aad7055

Nimmo, F., Hamilton, D. P., McKinnon, W. B., Schenk, P. M., Binzel, R. P., Bierson, C. J., et al. (2016). Reorientation of Sputnik Planitia implies a subsurface ocean on Pluto. *Nature*, *540*(7631), 94–96. https://doi.org/10.1038/nature20148

Nimmo, F., Umurhan, O., Lisse, C. M., Bierson, C. J., Lauer, T. R., Buie, M. W., et al. (2016). Mean radius and shape of Pluto and Charon from New Horizons images. *Icarus*, *287*, 12–29. https://doi.org/10.1016/j.icarus.2016.06.027

Robuchon, G., & Nimmo, F. (2011). Thermal evolution of Pluto and implications for surface tectonics and a subsurface ocean. *Icarus*, *216*(2), 426–439. https://doi.org/10.1016/j.icarus.2011.08.015

Rozel, A., Ricard, Y., & Bercovici, D. (2011). A thermodynamically self-consistent damage equation for grain size evolution during dynamic recrystallization. *Geophysical Journal International*, *184*(2), 719–728. https://doi.org/10.1111/j.1365-246X.2010.04875.x

Senft, L. E., & Stewart, S. T. (2008). Impact crater formation in icy layered terrains on Mars. *Meteoritics & Planetary Sciences*, *43*(12), 1993–2013. https://doi.org/10.1111/j.1945-5100.2008.tb00657.x

Senshu, H., Kuramoto, K., & Matsui, T. (2002). Thermal evolution of a growing Mars. *Journal of Geophysical Research*, *107*(E12), 5118–5121. https://doi.org/10.1029/2001JE001819

Stern, S. A., Bagenal, F., Ennico, K., Gladstone, G. R., Grundy, W. M., McKinnon, W. B., et al. (2015). The Pluto system: Initial results from its exploration by New Horizons. *Science*, *350*(6258). https://doi.org/10.1126/science.aad1815

Stern, S. A., Grundy, W. M., McKinnon, W. B., Weaver, H. A., & Young, L. A. (2018). The Pluto system after New Horizons. *Annual Review of Astronomy and Astrophysics*, *56*(1), 357–392. https://doi.org/10.1146/annurev-astro-081817-051935

Taylor, C., & Hood, P. (1973). A numerical solution of the Navier-Stokes equations using the finite element technique. *Computers & Fluids*, *1*(1), 73–100. https://doi.org/10.1016/0045-7930(73)90027-3

Trowbridge, A., Melosh, J., Steckloff, J., & Freed, A. (2016). Vigorous convection as the explanation for Pluto's polygonal terrain. *Nature*, *534*(7605), 79–81. https://doi.org/10.1038/nature18016

Vance, S., Bouffard, M., Choukroun, M., & Sotin, C. (2014). Ganymede's internal structure including thermodynamics of magnesium sulfate oceans in Contact with ice. *Planetary and Space Science*, *96*, 62–70. https://doi.org/10.1016/j.pss.2014.03.011

Vance, S., Panning, M., Stähler, S., Cammarano, F., Bills, B., Tobie, G., et al. (2018). Geophysical investigations of habitability in ice-covered ocean worlds. *Journal of Geophysical Research: Planets*, *123*(1), 180–205. https://doi.org/10.1002/2017je005341

Waite, W. F., Stern, L. A., Kirby, S. H., Winters, W. J., & Mason, D. H. (2007). Simultaneous determination of thermal conductivity, thermal diffusivity and specific heat in SI methane hydrate. *Geophysical Journal International*, *169*(2), 767–774. https://doi.org/10.1111/j.1365-246X.2007.03382.x

Zahnle, K., Schenk, P., Levison, H., & Dones, L. (2003). Cratering rates in the outer solar system. *Icarus*, *163*(2), 263–289. https://doi.org/10.1016/S0019-1035(03)00048-4